XL CILAMCE
IBERO-LATIN AMERICAN CONGRESS ON COMPUTATIONAL METHODS IN ENGINEERING
NOVEMBER 11-14, 2019
Praiamar Natal Hotel & Convention
Natal, RN-BRAZIL

GEOMETRICALLY NONLINEAR TRANSIENT ANALYSIS OF PLANE STEEL FRAMES USING A COROTATIONAL UPDATED LAGRANGIAN FORMULATION

Marília C. S. P. Salles
Harley F. Viana
Renata G. L. Silva
mariliapenido@yahoo.com.br
harley-viana@hotmail.com
rglanna.silva@gmail.com
Federal Center for Technological Education of Minas Gerais
7675 Amazonas Avenue, 30510-000, Minas Gerais, Brazil
Armando C. C. Lavall
lavall@dees.ufmg.br
Federal University of Minas Gerais
6627 Pres. Antônio Carlos Avenue, 31270-901, Minas Gerais, Brazil
Rodrigo S. Costa
rodrigo.sernizon@ufba.br
Federal University of Bahia
Augusto Viana Street, 40110-909, Bahia, Brazil

Abstract. The objective of this research is to present a study of the influence of the geometrical nonlinearities in the dynamic behavior of plane steel frames. The adopted geometrically nonlinear formulation is based on Euler-Bernoulli model and uses the updated Lagrangian description and the corotational approach to deduce the tangent stiffness matrix of the element with both fixed ends. The theory predicts that nodes will suffer large displacements and rotations, and the elements of the structure, large stretches and curvatures. The solution of the nonlinear equations of motion is achieved by combining the Newmark's implicit time integration method with the Newton-Raphson technique. The results of the performed analyzes showed a good agreement with the numerical solutions available in the literature, demonstrating the efficiency of the proposed method in obtaining the geometrically nonlinear dynamic behavior of steel structures.

Keywords: Geometrical nonlinearity, Second-order effects, Nonlinear transient analysis; Updated Lagrangian description; Corotational approach.

1 Introduction

Steel structures are generally designed for industrial and commercial buildings, since they have high strength-to-weight ratio and excellent ductility. In the case of light and slender structures, the influence of dynamic loads and second-order effects are more pronounced and, therefore, they cannot be neglected during the analysis. Additionally, several researches have been carried out in the field of structural analysis and it has been observed that only the linear static analysis may not be able to describe the real behavior of a structure submitted to the various external requests, especially in the case of atypical situations, such as earthquakes and strong wind gusts [1]. In these occasions, the structural elements can exhibit a diversity of behaviors, ranging from small strains to large displacements. Therefore, the correct design and prediction of such responses has led to the creation of consistent analytical models based on the finite element method.

These analytical models, using advanced analysis methods, can consider simultaneously several sources of the nonlinear behavior of structures as well as different types of loading, which leds to results more consistent with the real structural response and a less conservative design [1]. Regarding the nonlinear transient dynamic analysis, the conventional Lagrangian description has been extensively employed [2–5]. Nonetheless, this formulation requires an expressive modification in existing elemental hypothesis for nonlinear analysis [6]. By contrast, the adoption of a corotational formulation constitutes a good alternative to consider the geometric nonlinearity once it facilitates the decomposition of the element's motion into rigid body and pure deformational parts [7]. However, its domain of application is limited by a kinematic assumption that deformations must be small [8]. A number of interesting studies combining the corotational technique and the Lagrangian description have been published in the literature, as the works of Le et al. [9], Albinto et al. [10], da Silva et al. [11] and Huang et al. [12]. In this paper, the updated Lagrangian description is combined with the corotational approach in order to obtain the internal force vector and the tangent stiffness matrix.

An important feature in designing steel members and structures is the consideration of stability problems [13]. On the basis of this fact, researchers have proposed numerical formulations for nonlinear dynamic analysis of steel frames including second-order effects in terms of P-Δ and P-δ effects, as the studies presented by Chan and Chui [14], Liu et al. [13], Yu and Zhu [15], Nguyen and Kim [16], Silva et al. [17], and so on.

Nguyen and Kim [16] developed a simple numerical formulation based on the finite element method to be used in the second-order elastic dynamic analysis of space steel frames. The geometric nonlinearity was considered by using stability functions and geometric stiffness matrix. On the other hand, Yu and Zhu [15] applied the finite particle method for modeling the structural geometric nonlinearities in steel frames under dynamic loads. Since it is crucial to remove rigid body motion and rotation from the structural displacement, fictitious motion was used to address naturally the geometrical nonlinearity.

Liu et al. [13] proposed an efficient numerical procedure for time-history elastic analysis of three-dimensional steel frames using one-element-per-member model. The numerical simulation technique takes into account P-Δ and P-δ second-order effects, large global deflections and member deformations. The arbitrarily-located-hinge element proposed by Liu et al. [18–19] was used to explicitly simulate the initial member curvatures. The incremental secant stiffness approach is introduced to describe the kinematic motion of elements during the incremental-iterative procedure.

In order to deal with the effects of geometric nonlinearities, Cunha [20] employed the corotational description to the finite element method for 2D beam elements, based on the Euler-Bernoulli hypothesis. The tangent stiffness matrix was developed so that it can be decomposed into two parts, being one the material stiffness matrix and the other one called geometric stiffness matrix.

This paper concerns with a study of the dynamic behavior of plane steel frames, through time-domain integration, considering a geometrically nonlinear formulation. To this end, the numerical procedure for nonlinear static analysis proposed in da Silva et al. [11] is extended for nonlinear dynamic analysis of plane frames. However, in the present research, the shear deformation effect and

the material nonlinearity are not considered for comparison purposes. The adopted formulation employs an updated Lagrangian formulation and the corotational technique for the consistent deduction of the tangent stiffness matrix of the element with both fixed ends. The theory predicts that nodes will suffer large displacements and rotations, and the elements of the structure, large stretches and curvatures. The Newmark numerical integration scheme [21] is used in combination with the Newton-Rapshon iterative algorithm to solve the nonlinear dynamic equilibrium equations. In order to reduce computational effort in the simulations, the lumped mass matrix is adopted.

The described solution strategy was implemented in the PPLANLEP program, which is written in Fortran 90 language, and is capable to perform static and dynamic advanced analysis of framed steel structures. This program was developed by Lavall [22], adapted by Silva [23], who included the influence of semi-rigid connections and the shear deformations along the bars, and, then modified by Viana [1], who included the dynamic analysis in the structure of the program. The numerical responses obtained by the PPLANLEP program are compared with the numerical solutions available in the literature in order to demonstrate the efficiency and accuracy of the proposed analysis method.

2 Finite element model

The formulation for nonlinear static analysis of plane steel frames proposed by da Silva et al. [11] is used in the present study. Nonetheless, here it is employed the kinematic hypothesis of Euler-Bernoulli.

2.1 Coordinate systems

The 2D frame element with both fixed ends is shown in Fig. 1. The structural nodes have three degrees of freedom, namely, the displacements **u** and **v** along the axis **x** and **y**, respectively, and the rotation θ, positive when counter-clockwise. In the reference configuration, the chord between elements nodes has the length $\mathbf{l_r}$. On the chord a local reference coordinate system ($\mathbf{x_r}$,$\mathbf{y_r}$) is placed, with the origin at the center. The angle between the axis **x** and the chord is denoted by ϕ_r. At current configuration the chord between element nodes has length $\mathbf{l_c}$. A corrotational coordinate system ($\mathbf{x_c}$,$\mathbf{y_c}$) is defined on this chord, with the origin at the center, as indicate in Fig. 1. The angle between the axis **x** and the chord is now ϕ_c while the angle between the chord and the axis of the bar is denoted by α.

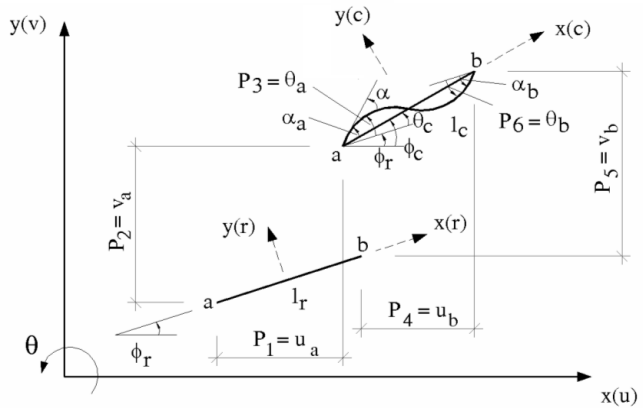

Figure 1. Finite element deformation for the fixed ends conditions

The degrees of freedom referent to the corotational system can be collected in a vector q_ω, where ω = 1, 2, 3:

$$\mathbf{q}^T = \{q_1; q_2; q_3\}. \tag{1}$$

The Cartesian degrees of freedom p_i (global system) are collected in the element's nodal

displacement vector, defined by

$$\mathbf{p}^{T} = \{u_a ; v_a ; \theta_a ; u_b ; v_b ; \theta_b\}. \tag{2}$$

The relations between natural and Cartesian degrees of freedom are important and listed below:

$$\begin{cases} q_1 = l_c - l_r \\ q_2 = \alpha_a = \theta_a - \theta_c = P_3 - \phi_c + \phi_r \\ q_3 = \alpha_b = \theta_b - \theta_c = P_6 - \phi_c + \phi_r \end{cases}. \tag{3}$$

being that:

$$\begin{cases} l_c = \left[(x_b - x_a + P_4 - P_1)^2 + (y_b - y_a + P_5 - P_2)^2 \right]^{1/2} \\ l_r = \left[(x_b - x_a)^2 + (y_b - y_a)^2 \right]^{1/2} \\ \sin\phi_c = \dfrac{y_b - y_a + P_5 - P_2}{l_c} \;; \quad \cos\phi_c = \dfrac{x_b - x_a + P_4 - P_1}{l_c} \\ \phi_c = \arctan\left(\dfrac{y_b - y_a + P_5 - P_2}{x_b - x_a + P_4 - P_1} \right); \quad \phi_r = \arccos\left(\dfrac{x_b - x_a}{l_r} \right) \end{cases}. \tag{4}$$

In Eq. (4), x_a, x_b, y_a and y_b are the element nodal coordinates at reference configuration.

The differential relations between the corotational coordinates and the Cartesian global coordinates can be written in a $\mathbf{B}_{3x6}$ matrix by deriving q_ω from p_i:

$$q_{\omega,i} = \mathbf{B} = \begin{bmatrix} -\cos\phi_c & -\sin\phi_c & 0 & \cos\phi_c & \sin\phi_c & 0 \\ -\dfrac{\sin\phi_c}{l_c} & \dfrac{\cos\phi_c}{l_c} & 1 & \dfrac{\sin\phi_c}{l_c} & -\dfrac{\cos\phi_c}{l_c} & 0 \\ -\dfrac{\sin\phi_c}{l_c} & \dfrac{\cos\phi_c}{l_c} & 0 & \dfrac{\sin\phi_c}{l_c} & -\dfrac{\cos\phi_c}{l_c} & 1 \end{bmatrix}. \tag{5}$$

where, comma indicates partial differentiation. Note that Greek indices range from 1 to 3, while Latin indices range from 1 to 6.

The second derivatives of q_ω with respect to p_i can be placed in three symmetrical matrices $\mathbf{G}_\omega$ (6x6) given by:

$$\mathbf{G}_1 = \frac{1}{l_c} \begin{bmatrix} \sin^2\phi_c & -\sin\phi_c\cos\phi_c & 0 & -\sin^2\phi_c & \sin\phi_c\cos\phi_c & 0 \\ & \cos^2\phi_c & 0 & \sin\phi_c\cos\phi_c & -\cos^2\phi_c & 0 \\ & & 0 & 0 & 0 & 0 \\ & & & \sin^2\phi_c & -\sin\phi_c\cos\phi_c & 0 \\ & \text{Symmetric} & & & \cos^2\phi_c & 0 \\ & & & & & 0 \end{bmatrix}. \tag{6}$$

$$\mathbf{G}_2 = \mathbf{G}_3 = \frac{1}{l^2_c} \begin{bmatrix} -2\sin\phi_c\cos\phi_c & (\cos^2\phi_c - \sin^2\phi_c) & 0 & 2\sin\phi_c\cos\phi_c & -(\cos^2\phi_c - \sin^2\phi_c) & 0 \\ & 2\sin\phi_c\cos\phi_c & 0 & -(\cos^2\phi_c - \sin^2\phi_c) & -2\sin\phi_c\cos\phi_c & 0 \\ & & 0 & 0 & 0 & 0 \\ & & & -2\sin\phi_c\cos\phi_c & (\cos^2\phi_c - \sin^2\phi_c)_c & 0 \\ & \text{Symmetric} & & & 2\sin\phi_c\cos\phi_c & 0 \\ & & & & & 0 \end{bmatrix} \tag{7}$$

2.2 Structural theory

Euler-Bernoulli hypothesis is assumes that cross-sections remain plane and perpendicular to the neutral axis after deformation. Displacement field of an arbitrary point in the beam element is defined if the axial displacement $u_c(x,y)$ and lateral displacement $v_c(x,y)$ of neutral axis are known, as well as the rotation of the transverse section, as depicted in Fig. 2.

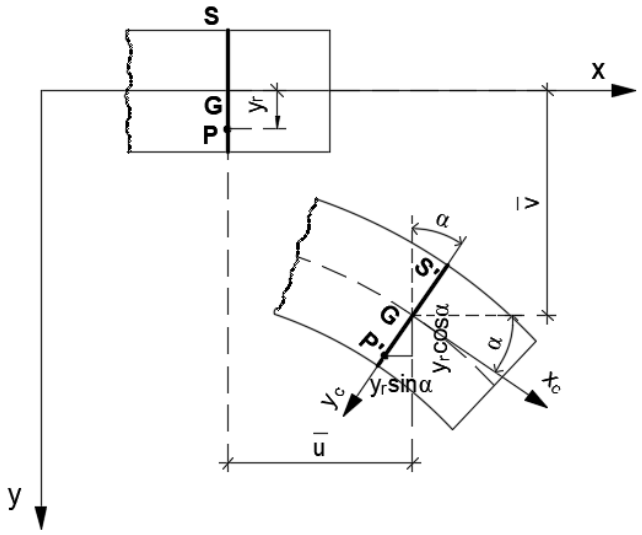

Figure 2. Displacement field considering the theory of Euler-Bernoulli

In the corotational system ($\mathbf{x_c}$, $\mathbf{y_c}$), u_c and v_c displacements represent the displacement fields of the point **P** of section **S**.

$$u_c(x,y) = \bar{u}_c(x) - y_r \sin\alpha\,. \tag{8}$$

$$v_c(x,y) = \bar{v}_c(x) - y_r(1-\cos\alpha)\,. \tag{9}$$

where, $\bar{u}_c$ and $\bar{v}_c$ are the displacements of the bar axis in the corotational system.

The rotation α of the cross sections results from the displacements $\bar{u}_c$ and $\bar{v}_c$ of the points on the bar's axis:

$$\alpha = \arctan\left(\frac{\bar{v}'_c}{1+\bar{u}'_c}\right). \tag{10}$$

Suppose that the rotation angle is small, Eq. (8) and Eq. (9) can be rewritten in the following form:

$$u_c(x,y) = \bar{u}_c(x) - y_r\alpha\,. \tag{11}$$

$$v_c(x,y) = \bar{v}_c(x) - y_r\frac{\alpha^2}{2}\,. \tag{12}$$

Based on the displacement field, the analytical expression of the deformation field for straight bars is deduced, getting to the following expression:

$$\varepsilon_x = \left(1+\bar{u}_c'\right)\sec\alpha - 1 - y_r\alpha'\,. \tag{13}$$

Adopting interpolation functions for displacements $\bar{u}_c$ and $\bar{v}_c$ of the bar's axis, it is obtained:

$$\bar{u}_c = q_1\Psi_1\,. \tag{14}$$

$$\overline{v}_c = \left(1 + \frac{q_1}{l_r}\right)\left(\Psi_2 q_2 + \Psi_3 q_3\right). \tag{15}$$

where

$$\begin{cases} \Psi_1(x_r) = \left(\dfrac{x_r}{l_r} + \dfrac{1}{2}\right) \\ \Psi_2(x_r) = \left(\dfrac{x_r^3}{l_r^2} - \dfrac{x_r^2}{2l_r} - \dfrac{x_r}{4} + \dfrac{l_r}{8}\right) \\ \Psi_3(x_r) = \left(\dfrac{x_r^3}{l_r^2} + \dfrac{x_r^2}{2l_r} - \dfrac{x_r}{4} + \dfrac{l_r}{8}\right) \end{cases}. \tag{16}$$

Deriving Eq. (14) and Eq. (15) and inserting into Eq. (10), the rotation α of the cross section can be calculated by

$$\alpha = \left(\Psi_2' q_2 + \Psi_3' q_3\right). \tag{17}$$

in which

$$\begin{cases} \Psi_2(x_r) = \left(\dfrac{3x_r^2}{l_r^2} - \dfrac{x_r}{l_r} - \dfrac{1}{4}\right) \\ \Psi_3(x_r) = \left(\dfrac{3x_r^2}{l_r^2} + \dfrac{x_r}{l_r} - \dfrac{1}{4}\right) \end{cases}. \tag{18}$$

The deformation of the bar's axis is given by $\overline{\varepsilon}_{xm}$, which is variable along its length. To facilitate the analytical development of the formulation, Lavall [22] adopted a constant value for $\overline{\varepsilon}$, represented by its mean value, given by:

$$\overline{\varepsilon}_{xm} = \frac{1}{l_r}\int \overline{\varepsilon}_x dx_r. \tag{19}$$

Although the hypothesis of small rotations of the elements' axis in relation to their chords is used, it does not prevent the occurrence of large curvatures as long as the elements are short. Thus, the expression for the deformation field is modified to:

$$\overline{\varepsilon}_{xm} = \frac{q_1}{l_r} + \left(1 + \frac{q_1}{l_r}\right)\left(\frac{q_2^2}{15} + \frac{q_3^2}{15} + \frac{q_2 q_3}{30}\right) - y_r\left(\Psi_2'' q_2 + \Psi_3'' q_3\right). \tag{20}$$

2.2 Equilibrium Equations

The virtual power principle is used in the development of the finite element stiffness:

$$\int_{V_r} \sigma_x \ \delta\varepsilon_x \ dV_r = P_i \delta p_i. \tag{21}$$

where dV_r is the volume element in the reference configuration, σ_x the normal stress, $\delta\varepsilon_x$ virtual longitudinal deformation and P_i are the element nodal forces.

The virtual longitudinal deformation is equal to:

$$\delta\varepsilon_x = \varepsilon_{x,\omega}\, q_{\omega,i}\, \delta p_i \,. \tag{22}$$

Therefore, the equilibrium equation of the element is given by:

$$P_i = Q_\omega q_{\omega,i} \,. \tag{23}$$

where Q_α is the element natural forces in corotational system:

$$Q_\omega = \int_{V_r} \sigma_x\, \varepsilon_{x,\omega} dV_r \,. \tag{24}$$

2.3 Element stiffness matrix

The derivative of P with respect to time can be given by:

$$\frac{dP}{dt} = \frac{\partial P}{\partial p}\frac{\partial p}{\partial t} = \mathbf{K_t}\frac{\partial p}{\partial t} \,. \tag{25}$$

where, $\mathbf{K}_t$ is the tangent stiffness matrix of element in Cartesian coordinates.

The components k_{ij} are obtained through differentiation of P_i with respect to Cartesian coordinate's p_j:

$$\frac{\partial P_i}{\partial p_i} = k_{ij} = q_{\omega,i}\, Q_{\omega,\beta}\, q_{\beta,j} + Q_\omega\, q_{\omega,ij} \,. \tag{26}$$

where $Q_{\omega,\beta}$ is the derivative of Q_ω with respect to q_β, which can be write as follows:

$$Q_{\omega,\beta} = \int_{V_r} \left(\varepsilon_{x,\omega}\, D\, \varepsilon_{x,\beta} + \sigma_x \varepsilon_{x,\omega\beta}\right) dV_r \,. \tag{27}$$

where D is the fiber's axial stiffness.

By Eq. (27) it is defined:

$$D_{\omega,\beta} = \int_{V_r} \varepsilon_{x,\omega}\, D\, \varepsilon_{x,\beta}\, dV_r \,. \tag{28}$$

$$H_{\omega,\beta} = \int_{V_r} \sigma_x\, \varepsilon_{x,\omega\beta}\, dV_r \,. \tag{29}$$

Then, a stiffness matrix for the element is established as:

$$k_{ij} = q_{\omega,i}\, D^f_{\omega,\beta}\, q_{\beta,j} + q_{\omega,i}\, H^f_{\omega,\beta}\, q_{\beta,j} + Q_\omega\, q_{\omega,ij} \,. \tag{30}$$

The constitutive part is represented by the first term of the Eq. (30), while the second and third terms represent the P-δ and P-Δ effects, respectively.

Finally, the symmetric tangent stiffness matrix (6x6) can be written as:

$$\mathbf{k_t} = \mathbf{k_M} + \mathbf{k_G} = \mathbf{B^T D\ B} + \mathbf{B^T H\ B} + Q_\omega \mathbf{G}_\omega \,. \tag{31}$$

in which $\mathbf{k_M}$ is the constitutive matrix and $\mathbf{k_G}$, the geometric matrix. As the material nonlinearity including gradual yielding of a steel beam–column member under axial force and bending moments is beyond the scope of this study, the constitutive matrix remains elastic.

3 Nonlinear dynamic solution procedure

The Newmark numerical integration scheme is combined with the Newton-Raphson method for the numerical integration of the nonlinear equations of motion. Thus, the incremental equation of motion of a structure is defined as:

$$\mathbf{M}\ddot{\mathbf{U}}^{(t+\Delta t)} + \mathbf{C}\dot{\mathbf{U}}^{(t+\Delta t)} + \mathbf{K}\mathbf{U} = \mathbf{F}_{ext}^{(t+\Delta t)} - \mathbf{F}_{int}^{t}. \tag{32}$$

where **M**, **C**, **K** are the mass, damping and tangent stiffness matrices, respectively; $\ddot{\mathbf{U}}$, $\dot{\mathbf{U}}$ are vectors of nodal point accelerations and velocities, respectively; $\mathbf{U}$ is the vector of nodal point displacement increments; $\mathbf{F}_{ext}$ is the applied external load vector and $\mathbf{F}_{int}^{t}$ is the nodal point force vector equivalent to the element stresses.

The Newmark's method consists in expressing the displacements and velocities according to finite difference approximations in the time domain, given by:

$$\mathbf{U}^{(t+\Delta t)} = \mathbf{U}^{t} + \Delta t\dot{\mathbf{U}}^{t} + \frac{\Delta t^2}{2}\left[(1-2\beta)\ddot{\mathbf{U}}^{t} + 2\beta\ddot{\mathbf{U}}^{(t+\Delta t)}\right]. \tag{33}$$

$$\dot{\mathbf{U}}^{(t+\Delta t)} = \dot{\mathbf{U}}^{t} + \Delta t\left[(1-\gamma)\ddot{\mathbf{U}}^{t} + \gamma\ddot{\mathbf{U}}^{(t+\Delta t)}\right]. \tag{34}$$

where γ and β are parameters that determine the stability and precision properties of the method.

From Eq. (33) it is obtained the incremental accelerations, given by:

$$\ddot{\mathbf{U}}^{(t+\Delta t)} = \frac{1}{\beta\Delta t^2}\Delta\mathbf{U} - \frac{1}{\beta\Delta t}\dot{\mathbf{U}}^{t} - \left(\frac{1}{2\beta}-1\right)\ddot{\mathbf{U}}^{t}. \tag{35}$$

Then, considering Eq. (35) into Eq. (34), the incremental velocities can be calculated from:

$$\dot{\mathbf{U}}^{(t+\Delta t)} = \frac{\gamma}{\beta\Delta t}\Delta\mathbf{U} - \left(\frac{\gamma}{\beta}-1\right)\dot{\mathbf{U}}^{t} - \Delta t\left(\frac{\gamma}{2\beta}-1\right). \tag{36}$$

Inserting Eq. (35) and Eq. (36) into Eq. (32), the equation that establishes the dynamic equilibrium of the structural system at **t + Δt** can be modified to:

$$\hat{\mathbf{K}}\,\Delta\mathbf{U} = \hat{\mathbf{F}}. \tag{37}$$

in which $\hat{\mathbf{K}}$ and $\hat{\mathbf{F}}$ are the effective stiffness matrix and the effective force vector, respectively, computed as:

$$\hat{\mathbf{K}} = \frac{1}{\beta\Delta t^2}\mathbf{M} + \frac{\gamma}{\beta\Delta t}\mathbf{C} + \mathbf{K}. \tag{38}$$

$$\hat{\mathbf{F}} = \mathbf{F}_{ext}^{(t+\Delta t)} + \mathbf{M}\left[\frac{1}{\beta\Delta t}\dot{\mathbf{U}}^{t} + \left(\frac{1}{2\beta}-1\right)\ddot{\mathbf{U}}^{t}\right] + \mathbf{C}\left[\left(\frac{\gamma}{\beta}-1\right)\dot{\mathbf{U}}^{t} + \Delta t\left(\frac{\gamma}{2\beta}-1\right)\ddot{\mathbf{U}}^{t}\right] - \mathbf{F}_{int}^{t}. \tag{39}$$

At the first iteration of each time step, the geometry, total displacement, velocity and acceleration are updated on the basis of the incremental displacement vector. For the second and subsequent iterations of each time step, the system of dynamic equations are solved under the effect of the residual force vector R, as follows:

$$\hat{\mathbf{K}}\,\delta\mathbf{U}_{k}^{(t+\Delta t)} = \mathbf{R}_{k}. \tag{40}$$

where $\mathbf{R}_k$ is computed at the unbalanced iterative step k, given as:

$$\mathbf{R}_{k}^{(t+\Delta t)} = \mathbf{F}_{ext}^{(t+\Delta t)} - (\mathbf{M}\ddot{\mathbf{U}}_{(k-1)}^{(t+\Delta t)} + \mathbf{C}\dot{\mathbf{U}}_{(k-1)}^{(t+\Delta t)} + \mathbf{F}_{int\,(k-1)}^{(t+\Delta t)}). \tag{41}$$

Thus, the incremental displacement vector is saved as:

$$\Delta\mathbf{U}_{k}^{(t+\Delta t)} = \Delta\mathbf{U}_{k-1}^{(t+\Delta t)} + \delta\mathbf{U}_{k}^{(t+\Delta t)}. \tag{42}$$

Using the incremental displacement vector, it is computed the velocities and accelerations at the unbalanced iterative step k. Once the convergence is achieved, the geometry, displacements, velocities and accelerations are saved for the next time step.

4 Numerical examples

A computer program written in Fortran 90 programming language was developed based on the present numerical procedure. Numerical examples are showed in order to evaluate the accuracy and efficiency of the proposed methodology in predicting the nonlinear elastic dynamic behavior of plane steel frames. In all analyzes, the lumped mass matrix is adopted and the effects of rotary inertia are neglected. The parameters γ and β of the Newmark method are considered equal to 0.5 and 0.25, respectively. Rayleigh proportional damping is not considered during the analysis.

4.1 Williams toggle frame

This problem, shown in Figure 3, has been solved analytically and experimentally by Williams [24]. This structure is commonly used by researchers to validate nonlinear numerical models and verify the efficiency of computational implementations. The structure consists of two members of rectangular sections with area of 1.1806 cm² and inertia of 0.036 cm^4. The frame is subjected to a concentrated load P (t) equal to 67 N. The structural members were discretized into 4 finite elements, and the cross section was divided into 10 slices. The modulus of elasticity and the volumetric mass adopted were 71.02 GPa and 2.7145 kNs^2/m^4, respectively. A constant time increment of 10^{-4} s and a tolerance of 10^{-5} for the displacements were adopted.

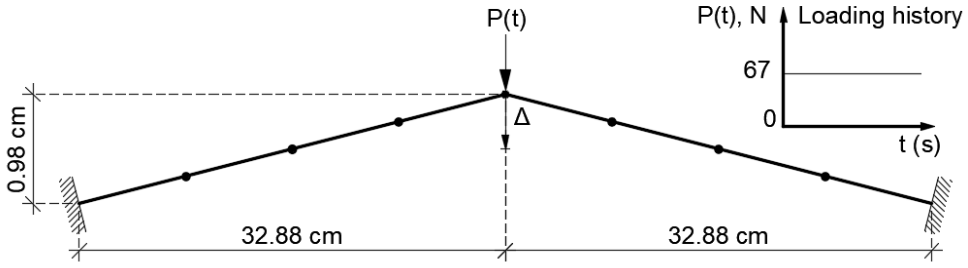

Figure 3. Williams toggle frame

The displacements at the top of the frame obtained by the proposed second-order analysis are closed with the displacements predicted by Chan and Chui [14], Silva [25] and SAP2000 commercial program, as plotted in Fig. 4. Comparing the numerical results provided by the second-order analysis with the first-order analysis, it can be observed that geometrical nonlinearities have a great influence on the structural behavior of this frame. The second-order effects cause a reduction in the structure's stiffness and, consequently, change de amplitude and period of vibration.

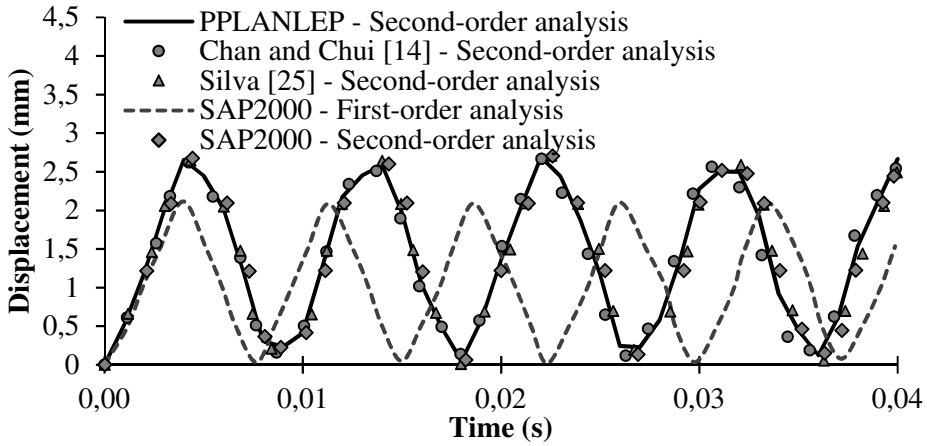

Figure 4. Displacement time response of Williams toggle frame

The small variation between the obtained results and results of other studies may be attributed to the difference in the numerical approach adopted. While Chan and Chui [14] and Silva [25] adopted a consistent mass matrix, the present work uses the lumped mass concept. As stated by Leitão [26] the natural period of vibration and the global second-order effects are influenced by the stiffness and mass matrices of the structure.

4.2 Cantilever under ramp-infinite duration load

A cantilever beam under a ramp-infinite duration load is shown in Fig. 5. This structure has been investigated by Behdinan et al. [27], Cunha [20] and other researchers. The elements have a cross-sectional area of 141.29 cm², inertia of 4162.32 cm^4, longitudinal modulus of elasticity equal to 206.85 GPa and linear density equal to 4.8807 x 10^{-7} kNs^2/cm^4. For this problem 10 elements were used in the discretization of the structure, and the cross section was divided into 20 slices. A constant time increment of 0.002 s and a tolerance of 10^{-4} for the displacements were adopted.

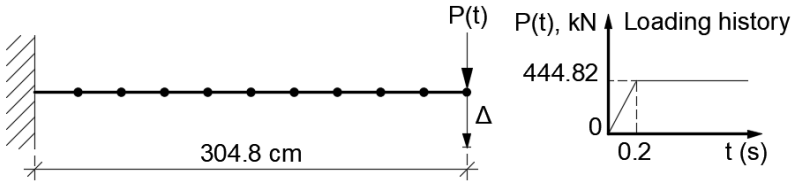

Figure 5. Beam geometry and loading history

The response obtained is in good agreement with those reported by Behdinan et al. [27] and Cunha [20], as depicted in Fig. 6. It can be noticed a regular oscillatory behavior regarding the amplitude and oscillation period from the instant 0.2 seconds, which is maintained until the end of the analysis.

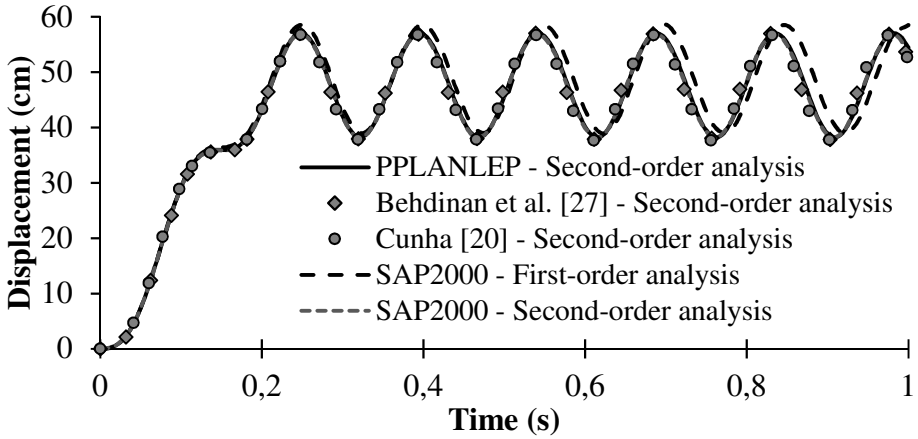

Figure 6. Time response of the cantilever under ramp-infinite duration load

It is observed that the linear and nonlinear responses have similar behavior; however, small differences between them are observed.

4.3 Portal steel frame with initial geometric imperfection

The objective of this example is to demonstrate the influence of the initial geometric imperfections on the dynamic response of steel frames. Figure 7 illustrates a portal frame with pinned supports. An initial geometric imperfection of column ψ of 1/200 is considered. The structure is subjected to two static loads of 200 kN and two concentrated masses acting on the top of the columns. All members of the structure are made of W8x48 steel profiles. In addition, the structure is subjected

to a horizontal impact load equal to 60 kN applied at the top of the left column. For all structural members, a longitudinal modulus of elasticity E of 205 GPa is adopted. The cross sections were discretized into 50 slices, 20 for each flange and 10 for the web. A time step of 0.001 s and a tolerance of 10^{-4} for the displacements were adopted in this analysis.

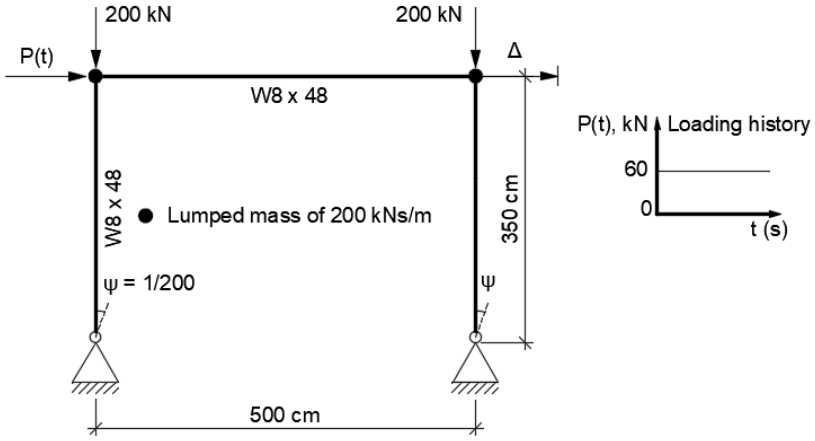

Figure 7. Pinned supported portal frame subjected to a horizontal impact load

Figure 8 shows the lateral displacement time-history at the top of the right column with the presence and absence of the initial geometric imperfections (GI). Analyzing the displacement time-history response it can be concluded that the initial geometric imperfections of the columns may increase the peak displacement of the structure. The geometric imperfections contribute to the second-order effects, resulting in a more flexible structure.

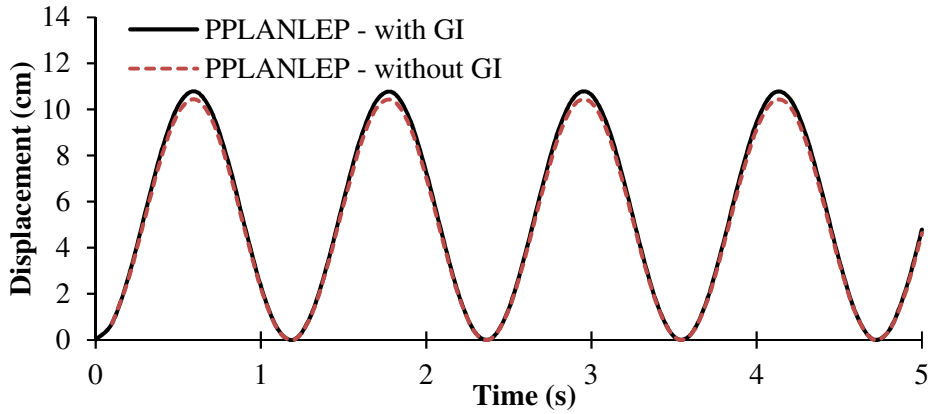

Figure 8. Displacement time-history response of the pinned supported portal frame

5 Conclusion

This paper presented a study of the dynamic behavior of plane steel frames, through time-domain integration, considering a geometrically nonlinear formulation that combines the corotational technique with the updated Lagrangian description. The theory predicted that nodes will suffer large displacements and rotations, and the elements of the structure, large stretches and curvatures. The Newmark time integration scheme combined with the Newton-Raphson iterative technique was chosen to solve the nonlinear incremental dynamic equilibrium equation in temporal domain. The lumped mass matrix was adopted and the effects of rotary inertia were neglected.

It was observed that the second-order effects, which includes both the P-Δ effect due to member chord rotation and the P-δ effect due to member curvature, can have a great influence on the structural behavior of frames, since they can cause a reduction in the structure stiffness. As a consequence, the results given by a second-order analysis may reveal a more flexible structure. Furthermore, it was concluded that the initial geometric imperfections may change the dynamic response of steel frames, in particular, the amplitude of vibration. Therefore, in order to precisely predict the behavior of steel frames, these attributes should be included during the analysis.

In all analyzes, it was found good agreement with the results provided by previous studies and the SAP2000 commercial program, confirming the efficiency of the formulation and numerical solution strategy adopted. Thus, it is believed that the present formulation may represent a valuable engineering tool for the nonlinear transient analysis of planar steel structures undergoing large displacements and rotations.

Acknowledgements

The authors gratefully acknowledge the financial support of this research given by the Minas Gerais State Agency for Research and Development – FAPEMIG and the Federal Center for Technological Education of Minas Gerais - CEFET-MG.

References

[1] H. F. Viana. Análise avançada dinâmica de pórticos planos de aço. Dissertação de Mestrado, Centro Federal de Educação Tecnológica de Minas Gerais, Belo Horizonte, 2019.

[2] K. Bathe, E. Ramm, and E. L. Wilson. Finite element formulations for large deformation dynamic analysis. *Int. J. Numer. Methods Eng.*, vol. 9, no. 2, pp. 353–386, 1975.

[3] M. Iura and S. N. Atluri. Dynamic analysis of finitely stretched and rotated three-dimensional space-curved beams. *Comput. Struct.*, vol. 29, no. 5, pp. 875–889, 1988.

[4] G. Jelenić and M. A. Crisfield. Interpolation of rotational variables in nonlinear dynamics of 3D beams. *Int. J. Numer. Methods Eng.*, vol. 43, no. 7, pp. 1193–1222, 1998.

[5] G. Jelenić and M. A. Crisfield. Geometrically exact 3D beam theory: implementation of a strain-invariant finite element for statics and dynamics. *Comput. Methods Appl. Mech. Eng.*, vol. 171, no. 1–2, pp. 141–171, 1999.

[6] H. Cho, H. Kim, and S. Shin. Geometrically nonlinear dynamic formulation for three-dimensional co-rotational solid elements. *Comput. Methods Appl. Mech. Eng.*, vol. 328, pp. 301–320, 2018.

[7] T.-N. Le, J.-M. Battini, and M. Hjiaj. A consistent 3D corotational beam element for nonlinear dynamic analysis of flexible structures. *Comput. Methods Appl. Mech. Eng.*, vol. 269, pp. 538–565, 2014.

[8] C. A. Felippa and B. Haugen. A unified formulation of small-strain corotational finite elements: I. Theory. *Comput. Methods Appl. Mech. Eng.*, vol. 194, no. 21–24, pp. 2285–2335, 2005.

[9] T.-N. Le, J.-M. Battini, and M. Hjiaj. Dynamics of 3D beam elements in a corotational context: A comparative study of established and new formulations. *Finite Elem. Anal. Des.*, vol. 61, pp. 97–111, 2012.

[10] J. C. R. Albino, C. A. Almeida, I. F. M. Menezes, and G. H. Paulino. Co-rotational 3D beam element for nonlinear dynamic analysis of risers manufactured with functionally graded materials (FGMs). *Eng. Struct.*, vol. 173, pp. 283–299, 2018.
[11] R. G. L. da Silva, A. C. C. Lavall, R. S. Costa, and H. F. Viana. Formulation for second-order inelastic analysis of steel frames including shear deformation effect. *J. Constr. Steel Res.*, vol. 151, pp. 216–227, 2018.
[12] C. C. Huang, F. Fujii, and K. M. Hsiao. An explicit algorithm for geometrically nonlinear transient analysis of spatial beams using a corotational total Lagrangian finite element formulation. *Comput. Struct.*, vol. 200, pp. 68–85, 2018.
[13] S.-W. Liu, R. Bai, and S.-L. Chan. Dynamic time-history elastic analysis of steel frames using one element per member. *Structures*, vol. 8, pp. 300–309, 2016.
[14] S.-L. Chan and P.-T. Chui. *Non-linear static and cyclic analysis of steel frames with semi-rigid connections*. Elsevier, 2000.
[15] Y. Yu and X. Zhu. Nonlinear dynamic collapse analysis of semi-rigid steel frames based on the finite particle method. *Eng. Struct.*, vol. 118, pp. 383–393, 2016.
[16] P.-C. Nguyen and S.-E. Kim. Nonlinear elastic dynamic analysis of space steel frames with semi-rigid connections. *J. Constr. Steel Res.*, vol. 84, pp. 72–81, 2013.
[17] A. R. D. Silva, E. A. P. Batelo, R. A. M. Silveira, F. A. Neves, and P. B. Gonçalves. On the Nonlinear Transient Analysis of Planar Steel Frames with Semi-Rigid Connections: From Fundamentals to Algorithms and Numerical Studies. *Lat. Am. J. Solids Struct.*, vol. 15, no. 3, 2018.
[18] S.-W. Liu, Y.-P. Liu, and S.-L. Chan. Direct analysis by an arbitrarily-located-plastic-hinge element—part 1: planar analysis. *J. Constr. Steel Res.*, vol. 103, pp. 303–315, 2014.
[19] S.-W. Liu, Y.-P. Liu, and S.-L. Chan. Direct analysis by an arbitrarily-located-plastic-hinge element—part 2: spatial analysis. *J. Constr. Steel Res.*, vol. 103, pp. 316–326, 2014.
[20] J. P. F. B. da Cunha. Análise estática e dinâmica de pórticos planos com o uso da formulação corrotacional. Dissertação de Mestrado, Universidade Federal de Goiás, 2018.
[21] N. M. Newmark. A method of computation for structural dynamics. *J. Eng. Mech. Div.*, vol. 85, no. 3, pp. 67–94, 1959.
[22] A. C. C. Lavall. Uma formulação teórica consistente para a análise não linear de pórticos planos pelo método dos elementos finitos considerando barras com imperfeições iniciais e tensões residuais na seção transversal. Tese de Doutorado, Universidade de São Paulo, São Carlos, 1996.
[23] R. G. L. Silva. Análise inelástica avançada de pórticos planos de aço considerando as influências do cisalhamento e de ligações semirrígidas. Tese de Doutorado, Universidade Federal de Minas Gerais, Belo Horizonte, 2010.
[24] F. W. Williams. An approach to the non-linear behaviour of the members of a rigid jointed plane framework with finite deflections". *Q. J. Mech. Appl. Math.*, vol. 17, no. 4, pp. 451–469, 1964.
[25] A. R. D. Silva. Sistema computacional para análise avançada estática e dinâmica de estruturas metálicas". Tese de Doutorado, Universidade Federal de Ouro Preto, Ouro Preto, 2009.
[26] F. F. Leitão, G. H. Siqueira, L. C. M. Vieira Jr, and S. J. C. Almeida. Análise dos efeitos globais de segunda ordem em estruturas irregulares em concreto armado utilizando o período natural de vibração. *Rev. IBRACON Estruturas e Mater.*, vol. 12, no. 2, pp. 408–428, 2019.
[27] K. Behdinan, M. C. Stylianou, and B. Tabarrok. Co-rotational dynamic analysis of flexible beams. *Comput. Methods Appl. Mech. Eng.*, vol. 154, no. 3–4, pp. 151–161, 1998.